

The 3D Resolution Power of the Full Tensor Gravity Gradient

José P. Calderón-Magallón*

*Department of Applied Geophysics, CICESE
Carretera Ensenada-Tijuana 3918, CP 22860,
Ensenada, BC, México
jcaldero@cicese.edu.mx*

Luis A. Gallardo

*Department of Applied Geophysics, CICESE
Carretera Ensenada-Tijuana 3918, CP 22860,
Ensenada, B.C., México
lgallard@cicese.mx*

SUMMARY

Airborne gravity tensor (or gravity gradient) surveying is one of the newest techniques for geophysical exploration. The rise in the acquisition of this data type is partially due to the fact that these data provide much more complete, extensive and higher resolution information of rock density distribution than conventional land gravity data. This has positioned Airborne Gravity Gradient (AGG) surveys among the geophysical services requested by mining companies, alongside aeromagnetic and radiometric surveys. The use of these data has been primarily to support geological mapping given the limited access to commercial software for quantitative depth interpretation. In particular, there has been a scarce development of AGG data inversion software, which has limited our understanding of the significance of these data for resolving three-dimensional subsurface targets. In this work we hypothesize that AGG data can provide more detailed information of the multidirectional variations of subsurface density. To prove this hypothesis, we developed conjugate gradient AGG-data inversion software for three-dimensional targets. This software was applied to synthetic data generated by several test assemblages of three-dimensional bodies and used to perform a Singular Value Decomposition (SVD) sensitive analysis to explore the actual resolution power of the different tensor data components and whether they are indeed superior to the conventional vertical gravity.

Key words: Gravity Gradient (GG), Conjugate Gradient, CG AGG, SVD.

INTRODUCTION

Since the early 20th century, gravity exploration has been extensively used in mineral and hydrocarbon exploration (see e.g. Nabighian *et al.*, 2005; Nabighian and Asten, 2002). Most gravity surveys have used gravity meters designed to differentially measure the vertical component of the gravity vector g_z . There have been alternative equipment to detect other field components. For instance, the first practical device to measure the horizontal component of the gravity field (the Torsion Balance) was designed in 1886 by von Eötvös and was successfully applied to detect the Nash Dome Field back in 1924 (cf. Zhdanov *et al.*, 2004). Despite this early success, economical application of Gravity Gradient (GG) fell out of favour and it was only after a recent two-decade development of several proprietary gradiometers (Dransfield, 2007; Dransfield and Lee, 2004; Jekeli, 1993; Murphy, 2004), which added the possibility of gravity surveys on aerial platforms, that GG mapping gained a renewed interest in exploration (Cevallos *et al.*, 2013; Jekeli, 2004).

The development of computational codes for the inversion of GG tensor data is an area that is receiving recent attention mainly by academic groups. Given the tensor characteristics of the GG data, progress in this direction has to account for full three-dimensional models which bring additional challenges typical on three dimensional optimization problems and, therefore, any development has to adhere closely to the massive processing strategies that these large-scale problems adopt (Moorkamp *et al.*, 2011; Zhdanov *et al.*, 2004). Despite these efforts, little attention has been given to the analysis of the actual resolution power of the different GG component data in three-dimensional scenarios.

In this work we suggest that the combined inversion of the various components of the GG data provides better resolution than conventional vertical gravity data and propose the development of an efficient conjugate gradient algorithm for the three dimensional inversion of massive GG data sets. We then apply the algorithm to two test experiments, which provide the sensitivity matrix required for a standard SVD resolution analysis of the problem.

The gravity gradient of a rectangular prism

We have a differential element located at the Cartesian coordinates $\mathbf{r}' = (x', y', z')$, and an observation point $\mathbf{r} = (x, y, z)$ (Figure 1). Following the integral form of Newton's Law, the potential field $U(\mathbf{r})$ produced by the mass contained within a volume V' is given by

$$U(\mathbf{r}) = -\gamma \iiint \frac{\rho(\mathbf{r}')}{|\mathbf{r} - \mathbf{r}'|} dv', \quad (1)$$

where γ is the gravitational constant of $6.674 \times 10^{-11} \text{ Nm}^2/\text{kg}^2$, $|\mathbf{r} - \mathbf{r}'| = ((x - x')^2 + (y - y')^2 + (z - z')^2)^{1/2}$ and $\rho(\mathbf{r}')$ is the mass density of the causative body enclosed. In geophysics we normally find analytical expressions developed for the vertical component $g_z(\mathbf{r})$.

In the particular case of a rectangular prismatic body of finite volume and uniform density $\rho(\mathbf{r}') = \rho$ (Figure 1), we may find the following expression for $g_z(\mathbf{r})$ [After *Banerjee and Gupta, 1977*]:

$$g_z(\mathbf{r}) = \gamma\rho \left[(x - x') \ln(y - y' + r) + (y - y') \ln(x - x' + r) - (z - z') \tan^{-1} \left(\frac{(x-x')(y-y')}{(z-z')r} \right) \right] \Big|_{x'_1}^{x'_2} \Big|_{y'_1}^{y'_2} \Big|_{y'_1}^{y'_2}, \quad (2)$$

where $r = |\mathbf{r} - \mathbf{r}'|$.

The mathematical representation of Gravity Gradient is performed using the Gravity Tensor (TG) which is the direct result of applying the second derivative of gravity potential $U(\mathbf{r})$. We represent the components of TG as follows

$$T_{\alpha\beta}(\mathbf{r}) = \frac{-\partial^2 U(\mathbf{r})}{\partial\alpha\partial\beta}, \quad (3)$$

where $\alpha, \beta = x, y, z$. Set a medium with homogeneous density; using equations (1) and (3), we obtain the general expression of the TG components

$$T_{\alpha\beta}(\mathbf{r}) = -\gamma \iiint_V \rho(\mathbf{r}') \frac{1}{|\mathbf{r} - \mathbf{r}'|^3} K_{\alpha\beta}(\mathbf{r} - \mathbf{r}') dv', \quad (4)$$

where $\rho(\mathbf{r}')$ is density of the body and $K_{\alpha\beta}$ is the Kernel of the function which has the form

$$K_{\alpha\beta} = \begin{cases} \frac{3(\alpha-\alpha')(\beta-\beta')}{|\mathbf{r}-\mathbf{r}'|^2} & \alpha \neq \beta \\ \frac{3(\alpha-\alpha')^2}{|\mathbf{r}-\mathbf{r}'|^2} - 1 & \alpha = \beta \end{cases} \quad (5)$$

where $\alpha, \beta = x, y$. The GG can be represented as a second order tensor (a square matrix) with nine components. Since it results from a scalar potential potential field, their cross-derivative components are the same, and the tensor reduces to only six independent components $T_{xx}, T_{yy}, T_{zz}, T_{xy} = T_{yx}, T_{xz} = T_{zx}, T_{yz} = T_{zy}$.

Using the equations (4) and (5) with a homogeneous density and following the procedure of Fosberg (1984), we obtain the general expression of the components of the gravity tensor

$$T_{\alpha\beta} = \gamma\rho \begin{bmatrix} \tan^{-1} \left(\frac{(z-z')(y-y')}{r(x-x')} \right) & -\ln(r + (z - z')) & -\ln(r + (y - y')) \\ -\ln(r + (z - z')) & \tan^{-1} \left(\frac{(x-x')(z-z')}{r(y-y')} \right) & -\ln(r + (x - x')) \\ -\ln(r + (y - y')) & -\ln(r + (x - x')) & \tan^{-1} \left(\frac{(x-x')(y-y')}{r(z-z')} \right) \end{bmatrix} \Big|_{x'_1}^{x'_2} \Big|_{y'_1}^{y'_2} \Big|_{y'_1}^{y'_2}. \quad (6)$$

Convolution-based 3D inversion of gravity gradient data

According to the superposition principle of gravity potential, we generalized the effect of a set of rectangular prisms as the summation of individual effects of each prism in a homogeneous medium. We express this generalization similar to the form of the equation (4); this expression indicates that, at a fixed z position and constant cell width, the derivative is the convolution of a characteristic 2D filter which does not need to be evaluated individually. This allows the efficient computation of sensitivities for thousands of observed data and horizontal cells. In fact, due to its symmetry, we only need to compute a single quadrant of the filter to cover the complete two-dimensional domain for each layer of cells.

3D INVERSION

We have the objective function to solve the inverse problem with the standard form

$$\phi = \|\mathbf{d}_{obs} - \mathbf{F}\mathbf{m}\|_{C_{dd}^{-1}}^2 + \|\mathbf{m} - \mathbf{m}_0\|_{C_{00}^{-1}}^2 + \alpha_p \|\mathbf{D}\mathbf{m}\|^2, \quad (8)$$

where C_{dd} is the covariance matrix of observed data, C_{00} is the covariance matrix, α_p is the penalty term. $\mathbf{D}\mathbf{m}$ is a regularization element that searches for the gradual lateral variation of the density inside the model, $\mathbf{F}\mathbf{m}$ is the model response, $\mathbf{m} - \mathbf{m}_0$ is the difference between density model \mathbf{m} and regularization model \mathbf{m}_0 . In our case, we follow a least squares formulation to find a model that minimizes the objective function based on a quadratic norm and obtain a lineal system of equations that can be solved through different numerical strategies.

We used the iterative Conjugate Gradient (CG) method to solve the resulting linear system of equations where we take full advantage of the convolution property of the gravity gradient for an ensemble of equally-sized cells.

SVD sensitive analysis

In general, the conventional analysis of resolution can barely distinguish the contribution of each element of the gravity tensor in the spatial domain. Instead, we used the Singular Value Decomposition (SVD) to characterize the whole sensitivity matrix before any regularization associated to the least square formulation, which enables a complete analysis of the pure data contribution. In this theory, a general rectangular $m \times n$ matrix A can be factorized in two orthogonal vector basis U and V in the form

$$A = UDV^T \quad (9)$$

where U is a $m \times m$ rectangular matrix, D is a partially diagonal matrix and V is a $n \times n$ rectangular matrix.

RESOLUTION TEST

Text Example I: Isolated L-test model source

The first model to analyze is an L-shaped source model formed with a group of prisms of equal size (1m x 1m x 2m) distributed along fifteen depth layers. For this model, we generated synthetic data using a density of 1 g/cm^3 for the cells localized inside the selected shape in the first three layers of prisms. For our particular choice of depths' it was expected that the resolution is best for the nearest model cells. We performed the inversion of the synthetic data using a damping parameter $\alpha_p = 10$ and an a priori model standard deviation of $\sigma_{00} = 0.1 \text{ gr/cm}^3$. This experiment resulted in the 3D model in Figure (2). The SVD for sensitive matrix of L-test model is shown in Figure 3a) and we can note the characteristic behaviour of the singular values for g_z and the individual elements of the gravity tensor. Figure 3b) shows maps of the different components of the GG and g_z fields for the singular vector associated to the largest singular value for the L-test model.

Text example II: Checker-board test model source

In a second experiment, we proposed a 3D checker board test model composed of $27 \times 27 \times 15$ rectangular prisms alternating their density from 1 g/cm^3 to -1 g/cm^3 every $3 \times 3 \times 3$ cells. For our inversion we selected a damping parameter $\alpha = 10$ and an a priori model standard deviation of $\sigma_{00} = 0.1 \text{ g/cm}^3$. For this experiment, we may note (Figure 4) that the resulting model was limitedly resolved for both the g_z and the various components of the gravity tensor. The SVD for the g_z and the various elements of the gravity tensor are shown in Figure 5a). Figure 5b) shows maps of the different components of the GG and g_z fields for the singular vector associated to the largest singular value for the L-test model.

DISCUSSIONS AND CONCLUSIONS

We can see that the application of the CG method to inversion of the gravity gradient and the g_z data, has good lateral resolution in the two examples; we may note, however that both data types have limited depth resolution (cf. Figures 2 and 4). In both cases only the upper layer is defined in any great detail. The rapid decay at depth can also be noticed in the SVD factorization, where the singular values show several step-like reductions amounting for half an order of magnitude decay for each step (Figures 3 and 5a). Results also show a slightly superior sensitivity to North-South property variations for all the tensor fields, which is even larger to that expected for vertical components. We thus conclude that gravity gradient data can provide more detailed information of the lateral variations of subsurface density which, however, decays rapidly at depth.

REFERENCES

- Banerjee, B., & S. P. D. Gupta 1977. Gravitational attraction of a rectangular parallelepiped, *Geophysics*, 42(5), 1053-1055.
- Cevallos, C., P. Kovac, & S. Lowe 2013. Application of curvatures to airborne gravity gradient data in oil exploration, *Geophysics*, 78(4), G81-G88.
- DiFrancesco, D., A. Grierson, D. Kaputa, & T. Meyer 2009. Gravity gradiometer systems - advances and challenges, *Geophys. Prospect.*, 57(4), 615-623.
- Dransfield, M. 2007. Airborne Gravity Gradiometry in the Search for Mineral Deposits, paper presented at Proceedings of Exploration 07: Fifth Decennial International Conference on Mineral Exploration.
- Dransfield, M., & J. B. Lee 2004. The FALCON® airborne gravity gradiometer survey systems, in R.J.L. Lane, Editor, Airborne Gravity 2004 - Abstracts from the ASEG-PESA Airborne Gravity 2004 Workshop: Geoscience Australia Record 2004/18, 7-14.
- Dransfield, M., & Y. Zeng 2009. Airborne gravity gradiometry: Terrain corrections and elevation error, *Geophysics*, 74(5), I37-I42.
- Geng, M., D. Huang, Q. Yang, & Y. Liu 2014. 3D inversion of airborne gravity-gradiometry data using cokriging, *Geophysics*, 79(4), G37-G47.
- Jekeli, C. 1993. A review of gravity gradiometer survey system data analyses, *Geophysics*, 58(4), 508-514, doi:doi:10.1190/1.1443433.

Jekeli, C. 2004. High-resolution gravity mapping: the next generation of sensors, in *State of the Planet: Frontiers and Challenges in Geophysics*, edited by R. S. J. H. C. J. Sparks, pp. 135-146.

Jekeli, C. 2006. Airborne gradiometry error analysis, *Surv. Geophys.*, 27(2), 257-275.

Martin, R., V. Monteiller, D. Komatitsch, S. Perrouty, M. Jessell, S. Bonvalot, & M. Lindsay 2013. Gravity inversion using wavelet-based compression on parallel hybrid CPU/GPU systems: application to southwest Ghana, *Geophys. J. Int.*, 195(3), 1594-1619.

Moorkamp, M., M. Jegen, A. Roberts, & R. Hobbs 2011. Massively parallel forward modeling of scalar and tensor gravimetry data, *Comput. Geosci.*, 36(5).

Murphy, C. A. 2004. The Air-FTGTM airborne gravity gradiometer system, edited, in R.J.L. Lane, Editor, Airborne Gravity 2004 - Abstracts from the ASEG-PESA Airborne Gravity 2004 Workshop: Geoscience Australia Record 2004/18, 7-14.

Nabighian, M. N., M. E. Ander, V. J. S. Grauch, R. O. Hansen, T. R. LaFehr, Y. Li, W. C. Pearson, J. W. Peirce, J. D. Phillips, & M. E. Ruder 2005. 75th Anniversary - Historical development of the gravity method in exploration, *Geophysics*, 70(6), 63ND-89ND.

Nabighian, M. N., & M. W. Asten 2002. Metalliferous mining geophysics - State of the art in the last decade of the 20th century and the beginning of the new millennium, *Geophysics*, 67(3).

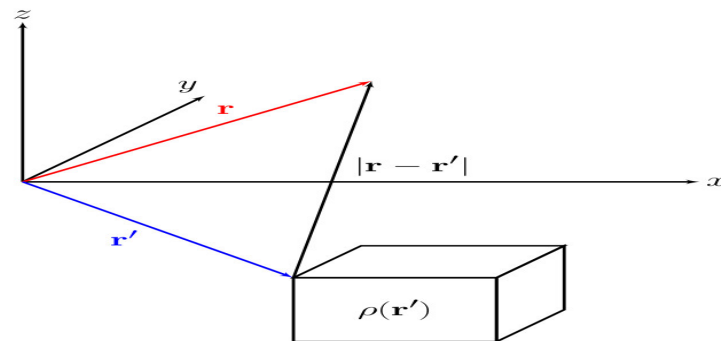


Figure 1. Illustration of the basic rectangular prism used to model gravity tensor data. Note that the lateral extensions of the prism are assumed parallel to the reference system.

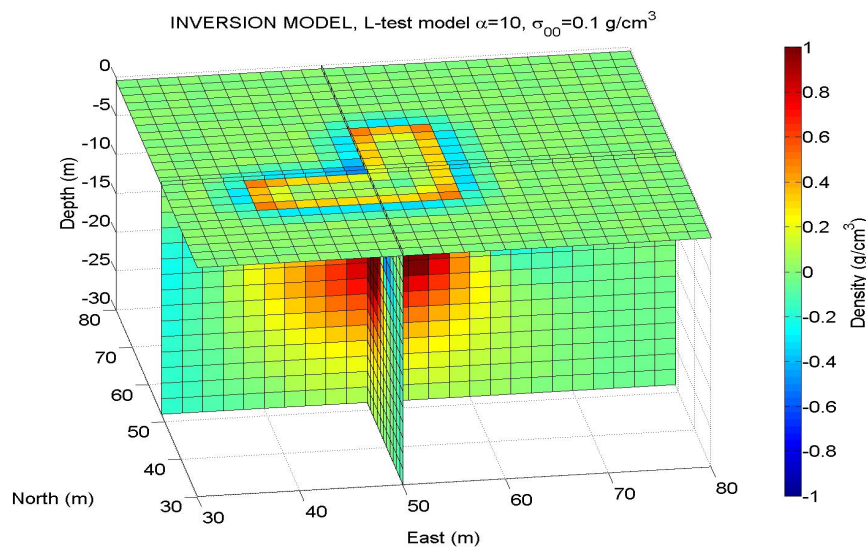


Figure 2. Test model obtained by the joint inversion of TG and g_z data generated by a L-shape body placed within in the top three layers. Density color scale is shown from -1 to 1 g/cm^3 .

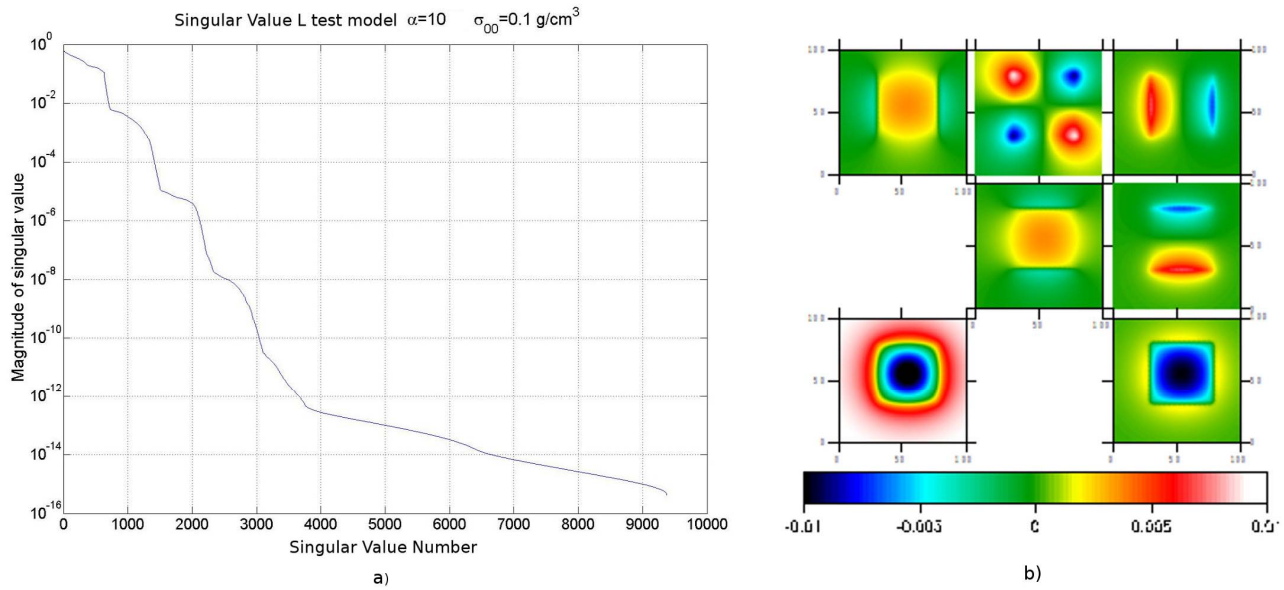


Figure 3. a) Singular values obtained for the sensitivity matrix of a L-test model. The values are ordered from the largest to the smallest and data sensitivity includes both g_z and GG data. Note that the decay of the values is given by continuous steps where the values decay by half an order of magnitude at every 729 values (amount of horizontal cells per model layer). **b)** Maps of the different components of the GG and g_z fields for the singular vector associated to the largest singular value for the L-test model. It is noticeable that the data are mainly sensitive to North-South variations for all the fields rather than vertical fields.

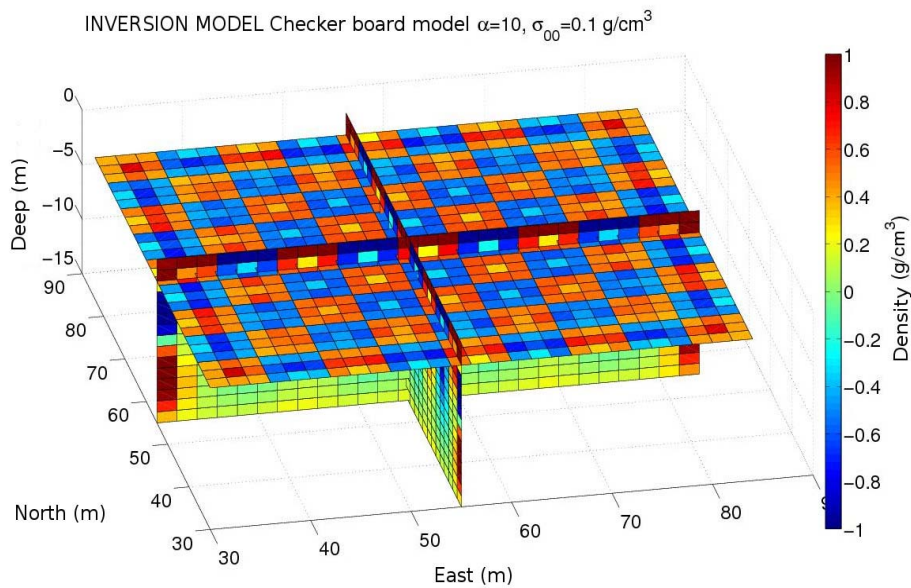


Figure 4. Optimal model obtained by the joint inversion of TG and g_z data generated by a checker-board test model with density values ranging -1 to 1 g/cm^3 . Depth layers are 1 m thick.

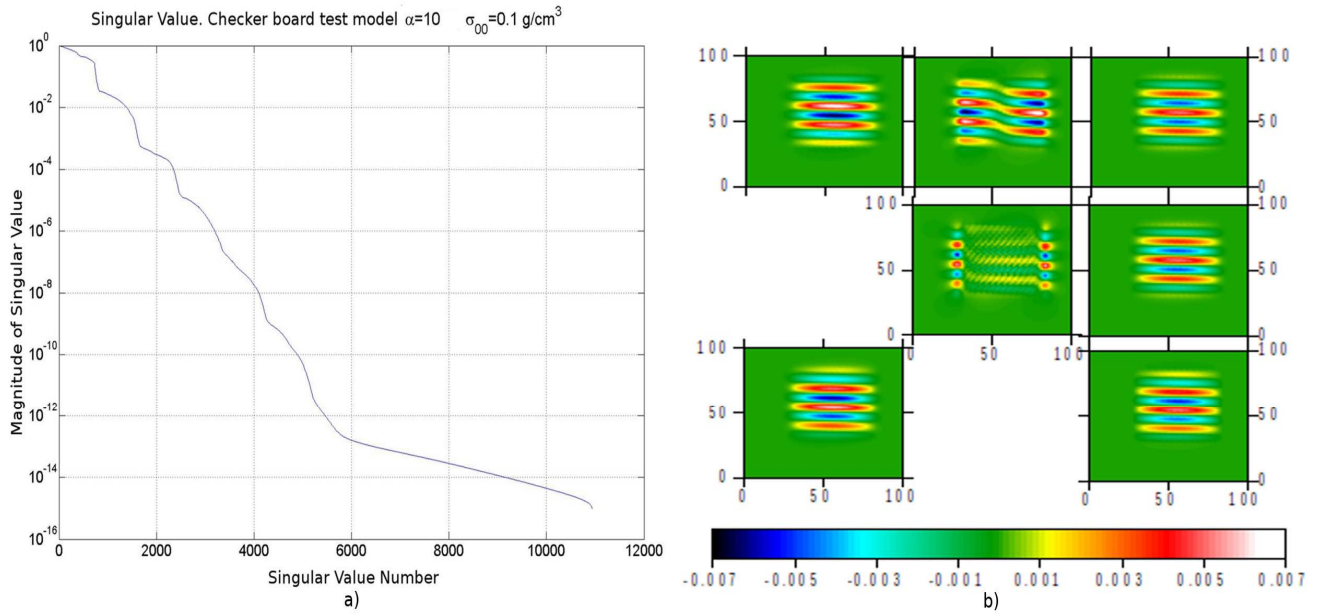


Figure 5. a) Singular values obtained for the sensitivity matrix of a 27x27x15 cell model. The values are ordered from the largest to the smallest and data sensitivity includes both g_z and GG data. Note that the decay of the values is given by continuous steps where the values decay by half an order of magnitude at every 729 values (amount of horizontal cells per model layer). b) Maps of the different components of the GG and g_z fields for the singular vector associated to the largest singular value for the test model of 27x27x15 cells. It is noticeable that the data are mainly sensitive to North-South variations for all the fields rather than vertical fields.